Beam filtration for object-tailored X-ray CT of multi-material cultural heritage objects

Kiss, M.B.; Bossema, F.G.; Laar, P.J.C. van; Meijer, S.; Lucka, F.; Leeuwen, T. van; Batenburg, K.J.

Kiss *et al. Heritage Science* (2023) 11:130
https://doi.org/10.1186/s40494-023-00970-z

Heritage Science

RESEARCH

Open Access

Beam filtration for object-tailored X-ray CT of multi-material cultural heritage objects

Maximilian B. Kiss[1*], Francien G. Bossema[1,2], Paul J. C. van Laar[1,2,3], Suzan Meijer[2], Felix Lucka[1], Tristan van Leeuwen[1,4] and K. Joost Batenburg[1,5]

Abstract

Computed tomography (CT) is a powerful non-invasive tool to analyze cultural heritage objects by allowing museum professionals to obtain 3D information about the objects' interior. These insights can help with the conservation or restoration of the objects, as well as provide contextual information on the objects' history or making process. Cultural heritage objects exist in a wide variety and have characteristics which present challenges for CT scanning: multi-scale internal features, a diversity of sizes and shapes, and multi-material objects. Because X-ray absorption is related to the density, thickness of the material, and atomic composition, the challenges are greater when the object consists of multiple different materials with varying densities. This is especially true for cases with extreme density contrasts such as that between metals and textiles. An untailored acquisition of CT scans of multi-material objects can lead to reduced image quality and heavy visual errors called image artifacts, which can influence the perception or representation of information. A tailored acquisition can reduce these artifacts and lead to a higher information gain. In this work, we firstly discuss how the X-ray beam properties and the beam-object interaction influence CT image formation and how to use filters to manipulate the emitted X-ray beam to improve image quality for multi-material objects. We showcase that this can be achieved with limited resources in a low-cost DIY fashion with thin sheets of metal as filters, 3D-printed filter frames and a filter holder. Secondly, we give a qualitative analysis of the influence of the CT acquisition parameters illustrated with two case study objects from the textile collection of the Rijksmuseum, Amsterdam, The Netherlands. With this we provide insights and intuitions on tailoring the CT scan to the cultural heritage objects. Thirdly, we extract a general concept of steps for museum professionals to design an object-tailored CT scan for individual cases.

Keywords X-ray computed tomography, Cultural heritage, Metal artifacts, Beam hardening, Beam filtration, Artifact reduction

Introduction

Computed Tomography (CT) is a non-invasive X-ray imaging technique. The scanning setup consists of an X-ray source, a detector and a rotation stage on which the object of interest is mounted. A single X-ray image, also called radiograph or projection, is created by shooting X-rays at the detector, with the object in between. Part of the radiation is attenuated by the object, based on material properties such as density, thickness, and atomic composition. The resulting image on the detector is an overlay of the materials in the direction of the X-rays. For a CT scan, the object is rotated, while 2D X-ray images

*Correspondence:
Maximilian B. Kiss
maximilian.kiss@cwi.nl
[1] Computational Imaging, Centrum Wiskunde & Informatica, P.O. Box 94,079, 1090, GB, Amsterdam, The Netherlands
[2] Conservation and Science Department, Rijksmuseum, P.O. Box 74,888, 1070, DN, Amsterdam, The Netherlands
[3] NOVA School of Science and Technology, Universidade NOVA de Lisboa, Largo da Torre, 2829–516 Caparica, Portugal
[4] Mathematical Institute, Utrecht University, P.O. Box 80,010, 3508, TA, Utrecht, The Netherlands
[5] LIACS, Leiden University, P.O. Box 9512, 2300, RA, Leiden, The Netherlands

are taken at small angular intervals. Afterwards, computer algorithms are used to create a tomographic reconstruction of the data. This is a 3D representation of the interior of the object, a grey scale map where the pixel/CT values represent the relative densities of materials in the object. This 3D image can for example be viewed as a stack of 2D images, called slices, which show a virtual cut through the object [1, 2]. Since the development of X-ray CT, its applications broadened from the medical sector to various other fields, e.g. manufacturing industry, food industry, and material sciences [3].

Computed tomography in cultural heritage

Computed tomography has also proved to be a powerful non-invasive tool to analyse cultural heritage objects [4]. It has been successfully applied to a variety of such objects over the past decades: for example, wooden statues for dendrochronology research [5] and large wooden objects [6, 7], Egyptian funerary masks [8], antique glass [9], musical instruments [10, 11], ancient basketry [12], anthropological studies [13, 14] and historical paintings [15, 16]. In cases where it is not possible to see the interior of an object using visual inspection, CT enables museum professionals to obtain 3D information about the interior of the object. In particular, CT scanning gives a much more detailed overview than radiography because it is three-dimensional, allowing to isolate specific features and parts by virtually cutting through the object in any location and direction. These insights can help with the conservation or restoration of the objects, as well as provide contextual information on the object's history or making process [17].

Challenges specific to CT in cultural heritage

Cultural heritage objects exist in a wide variety and have characteristics which present challenges for CT scanning: multi-scale internal features, a diversity of sizes and shapes, and multi-material objects [18]. The last challenge is even greater when the multiple different materials of the object have varying densities, especially when one of the materials is a metal [19]. A multi-material object might be for example made out of fabric, leather, metal thread and different kinds of beads as well as designed in a multi-layered way. Hidden intermediate layers that could give insight into the object's history and making process might be difficult to analyse. Additionally, the actual dimensions and characteristics of these layers are usually not visible from the outside. Investigating these characteristics using X-ray radiographs (2D X-ray projections) will only give a limited amount of information, whereas CT-scanning will be more informative. Acquiring CT scans of these objects with standard lab/museum CT scanners in an untailored way yields images with heavy visual errors (see Fig. 1) called image artifacts.[1]

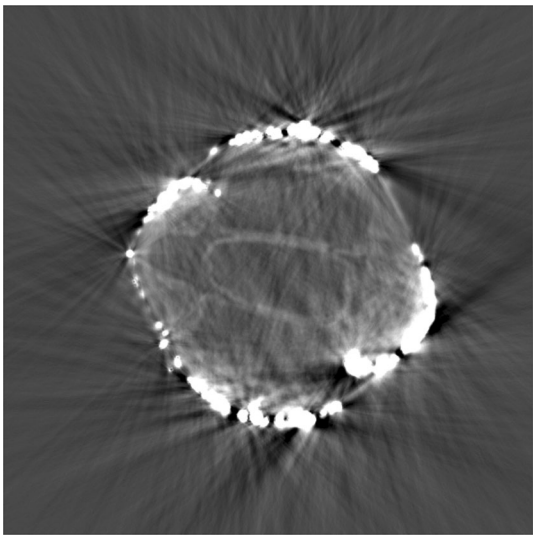

Fig. 1 Heavy visual errors (image artifacts) exhibited by an untailored CT scan of a multi-material cultural heritage object

Difference to medical CT challenges

Although both the medical and the cultural heritage sector need an acceptable image quality for interpretation and face similar challenges in the CT acquisition, they are fundamentally different [4, 20]. In medical CT scans the scanned subjects (humans) are similar with respect to their anatomy and the material composition. The human body is generally more homogeneous with respect to its density distribution compared to cultural heritage objects. Although metals may be present in the form of prostheses, these are confined to specific regions whereas metals in cultural heritage can also occur scattered throughout the object. Furthermore, the energy regime of the photons is different and improvements to medical CT have been extensively researched, e.g. the tuning of tube voltage and current, using filters and software-based artifact correction algorithms [21]. Lastly, the medical sector lacks an extensive adaptability of acquisition parameters since commercial CT scanners are used that have a limited number of adjustable settings. In contrast, objects scanned in the cultural heritage sector are all different in size and material composition and there is limited knowledge on what is in the object and what it is made of. As CT scans are typically carried out with laboratory-setups, the acquisition parameters can be adjusted

[1] The word artifact is used in this paper only in reference to visual errors in CT images, not in reference to an object shaped by human workmanship (sometimes referred to as 'artefact').

and researchers can interactively investigate the effect of these parameter choices [22]. We will show that the aforementioned challenges can be overcome by tailoring the acquisition parameters to the object under study. This enables not only cleaner and more expressive 2D X-ray projections (radiographs) but also more informative reconstructions. Therefore, it is advisable to analyse the objects to be scanned for taking possible causes of image artifacts into account (cf. "Background" section).

Contributions

The contributions of this work are as follows: Firstly, we briefly introduce several of the key factors that influence computed tomography image formation in the context of cultural heritage objects to make this work accessible to a broad audience including museum professionals as well as X-ray imaging specialists. We address the underlying physics and discuss the use of filters to manipulate the emitted X-ray beam to improve image quality for these multi-material objects. This can be achieved with limited resources in a low-cost DIY fashion as described in the "Hard- and software" section. Secondly, we give a qualitative analysis of the influence of the CT acquisition parameters illustrated with two case study objects from the textile collection of the Rijksmuseum, Amsterdam, The Netherlands (cf. "The case studies" section), which were scanned at the FleX-ray Lab of the Centrum Wiskunde & Informatica, Amsterdam, The Netherlands. With this we provide insights and intuitions on how to design a CT scan and on choosing suitable acquisition parameters, illustrated by these case studies. Thirdly, we extract a general concept of steps for museum professionals to design an object-tailored CT scan for individual cases.

As this paper is positioned at the interface between scientific imaging and cultural heritage, it will be necessary to sometimes make certain obvious statements, to ensure a common ground of understanding between professionals with different backgrounds and technical knowledge.

Background

In this section we will address how the multi-material nature of cultural heritage objects presents a challenge for CT imaging that can lead to reduced image quality and errors in the perception or representation of information called image artifacts. These image artifacts can hinder effective reconstruction and visualization of the acquired data but also limit the information or complicate its interpretation. The three main factors that contribute to lower image quality are (i) the polychromatic X-ray spectrum and metal artifacts; (ii) the contrast between materials; (iii) noise and detector saturation.

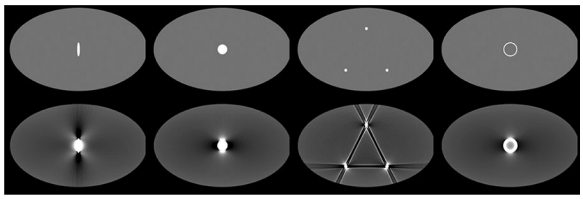

Fig. 2 Simulated scans without (top row) and with (bottom row) beam hardening, showing that dark streaks occur along the lines of greatest attenuation, and bright streaks occur in other directions. Also note the subtle "shadows" beneath the surface, which is caused by beam hardening and is called cupping artifact. Reprinted with permission from [44]

Polychromatic X-ray spectrum and metal artifacts

The X-ray beam used for CT imaging commonly has a polychromatic nature, meaning that the beam emitted from the X-ray source emits a spectrum of photon energies. Exceptions for these polychromatic beams can be found in specialized synchroton facilities which generate a monochromatic beam, with photons of one specific energy. Furthermore, the attenuation of X-ray photons traversing a material is energy dependent. The attenuation coefficient of materials commonly present in cultural heritage objects decreases as the photon energy increases. [23]

The standard computational models used in CT imaging rely on the assumption that the X-ray beam is monochromatic, assigning a single attenuation coefficient to each material. However, the polychromatic nature of the X-ray beam leads to an error in the attenuation coefficients and the linear relationship between them and the material thickness due to the energy-dependence of the attenuation. This is called beam hardening and causes a variety of image artifacts [24, 25]. Two signs of these beam hardening image artifacts are "cupping" and "streaking". When regions in the scanned sample appear brighter (higher density) at the edges than at the center (decreased brightness) this is called a cupping artifact. Streaking artifacts show as dark and light streaks around structures with a high density. Visual examples of both image artifacts can be found in Fig. 2.

An extreme example of such dense materials are metals. The attenuation coefficients of metals are much higher than those for lighter materials such as ceramics, wood, or textiles and can lead to incomplete attenuation profiles. In particular, around the K-edge of metal elements - a sudden increase in X-ray absorption when the energy of the X-rays is just above the binding energy of the innermost electron shell - the absorption properties change substantially and cause errors in the reconstructed CT image. Metal objects in the field of view can therefore also lead to severe streaking image artifacts.

This is due to a combination of beam hardening and photon starvation but can also originate in extreme contrasts within the radiographs. Photon starvation is an effect where the attenuation of a material is so high that almost no signal for a given X-ray beam is detected behind the object in some of the orientations. Without a measured signal, star-like streaks originating in the metal structure appear in the CT reconstruction (cf. Fig. 2).

Contrast between materials

The concept of contrast is generally hard to measure and quantify. A common aim when conducting CT scans is to have a high difference in absorption between the features of interest inside the object and their surroundings, including the scanning medium (air, sand, water, etc.) [26]. A high contrast-to-noise ratio (CNR) enables visual interpretability and might be very case-dependent. For many materials common in cultural heritage the absorption curve has a steeper slope for lower photon energies. Therefore, lower photon energies in the X-ray beam enable more contrast between the different materials [27]. This property can be utilized to achieve higher contrast between the different materials by creating a beam spectrum with photons whose energy is low but sufficient to penetrate the object.

Noise and detector saturation

In a CT scan, all angular projections are acquired using a fixed exposure time and source current, which jointly determine the beam intensity that reaches the detector after interacting with the object. When acquiring the projection images, it must be ensured that for each individual projection the detector measures a sufficient signal across the X-ray image, while at the same time not saturating the detector at any particular location.

For a given exposure time, the maximum source intensity is limited by the values measured at the detector without an object present between the X-ray source and the detector (the so-called "flat-field"), which should not trigger detector saturation. The minimum suitable values for intensity and exposure time can be found by rotating the object to find the line of sight that has the largest attenuation, resulting in the lowest signal at the detector across the full CT scan. As a rule of thumb, this value should be at least a factor 2–3 greater than the signal measured with the source turned off (the so-called "dark-field") or around 5% of the total count range [28].

It is noteworthy that the photons in the low-energy range of the spectrum contribute to detector saturation, while at the same time may hardly contribute to the actual signal measured while scanning the object. Filtering out these photons at the source can therefore be useful in improving penetration of the object while avoiding detector saturation. Within these limits, increasing the beam intensity will lead to a higher signal-to-noise ratio (SNR) of the projections, resulting in reduced noise in the reconstructed CT image.

Methods

In this section we describe the concepts and resources used for the investigation of the two case study objects.

Concept of beam filtration

As described in the "Background" section, the interplay between a broad beam spectrum and the energy-dependent absorption of the sample's materials can create a range of image artifacts. In this section, we discuss the concept of beam filtration which is the placement of materials into the X-ray beam that modify the spectrum of the beam. We describe how beam filtration can reduce the low-energy portion of the X-ray spectrum, commonly referred to as "pre-hardening the beam", and allows mainly higher energy X-rays to pass through the scanned object. This narrows the standard beam spectrum for CT imaging as well as shifts its mean photon energy towards higher energies, minimizing image artifacts due to beam hardening and avoiding saturation of the detector.

The filtration of the beam typically happens at or near the X-ray tube window in the direct path of the X-ray beam. The filters applied to the X-ray beam are commonly thin sheets of metal, such as aluminum (Al), copper (Cu), iron (Fe), tin (Sn), and tungsten (W), but studies have shown that combination filters of different materials and thicknesses are even more effective in reducing the image artifacts [29–31]. These compound filters combine the different attenuation characteristics of various materials and result in more effective filtering by reducing intensity of low-energy photons over a wider band. One well-established compound filter is the so-called Thoraeus filter, which consists of tin, copper and aluminum at varying thicknesses. This compound filter can effectively filter out photons carrying an energy of 1.5–70 keV [32]. In practice, very low energy photons are filtered out already by the X-ray tube exit window itself. In Fig. 3 the beam spectra of a tungsten target X-ray source operated at different tube voltages and with different filters are shown.

Hard- and software

This explorative study is a collaborative work of conservators, curators and researchers from the Rijksmuseum, Amsterdam, and CT imaging scientists from the Centrum Wiskunde & Informatica (CWI) Amsterdam. All scans were conducted in the custom-built FleX-ray Lab at CWI, which contains a highly flexible X-ray CT scanner, developed by TESCAN XRE NV [33]. Generally,

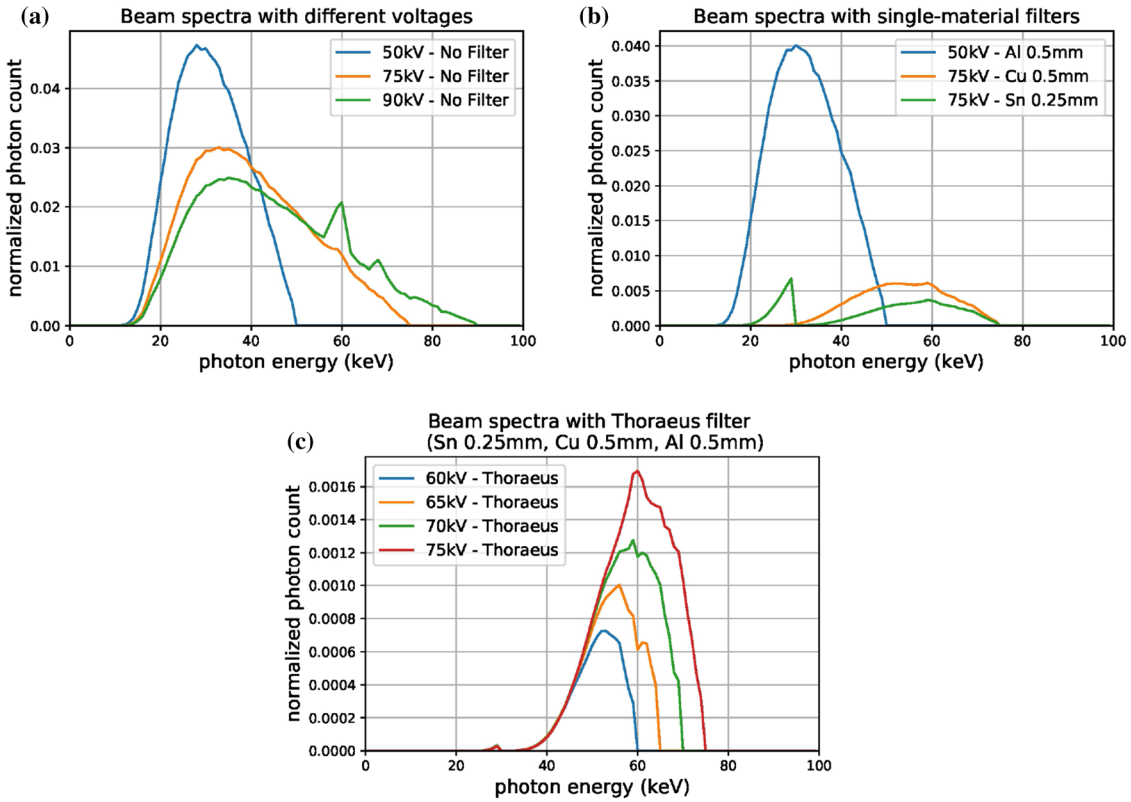

Fig. 3 Beam spectra of a tungsten target X-ray source with an X-ray exit window made of 300 µm Beryllium simulated by TASMIP software [45]. **a** at different tube voltages 50 kV, 75 kV, 90 kV (A continuous distribution of energies composed of Bremsstrahlung photons and discrete lines of characteristic radiation [for tungsten 58 and 69 keV] can be seen. The maximal photon energy of the beam spectrum is determined by the tube voltage. This maximal energy though is hardly represented by photons, while most of the photons are at roughly one third of this peak energy); **b** at tube voltages of 50/75 kV filtered with either aluminum, copper or tin of varying thicknesses (see legend); **c** at varying tube voltages 60, 65, 70, 75 kV filtered with a Thoraeus compound filter of Sn 0.25 mm, Cu 0.5 mm, Al 0.5 mm

this laboratory is used to conduct proof-of-concept studies in the field of mathematics and computer science [34]. The scanner has three main components: (i) a cone-beam microfocus X-ray point source emitting polychromatic X-rays between 20 keV and 90 keV with a tube current between 10 µA and 1000µA; (ii) a rotation stage, on which samples of different sizes (up to 40 cm × 40 cm × 40 cm) can be mounted; and (iii) a CMOS (complementary metal-oxide semiconductor) flat panel detector with a CsI(Tl) scintillator (Dexella 1512NDT, [35]) with 1536 x 1944 pixels, 74.8µm^2 each, onto which the X-rays are projected. The off-set counts ("dark currents") and the maximal readout of this detector are given by $\sim 1,000$ and 65,000 counts respectively. Translation stages enable all three components to move independently from one another. An image of the scanning set-up is shown in Fig. 4.

We point out that the maximum tube voltage available for the FleX-ray scanner is lower than other commercial systems that range between 40 and 225 kV. The purpose of this paper however is to investigate the two case study objects and to give general guidance on designing object-tailored CT scans. Particular results will be dependent on the individual scanners used. Specifically, the available maximum tube voltage will have a strong impact on the ability to penetrate the objects. For some of the experiments in this paper the maximum tube voltage of the FleX-ray scanner limits the shaping of the beam spectrum tailored to the given materials in the objects but because of their small thickness, it was possible to reduce the metal artefacts sufficiently to reveal the layers and other materials in the object.

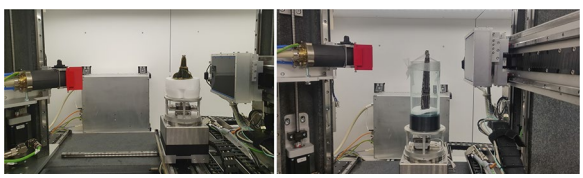

Fig. 4 Scanning setup for the case study objects in the FleX-ray scanner

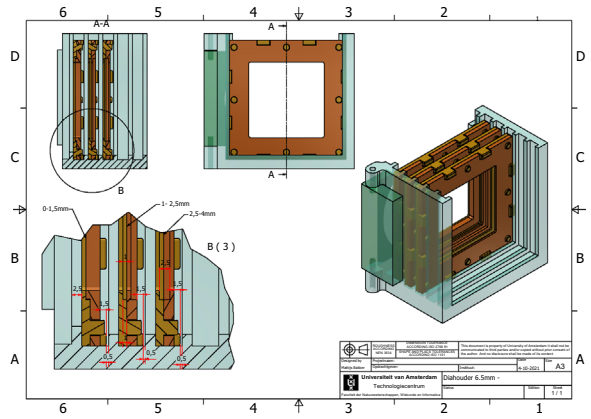

Fig. 5 Technical drawings of the 3D-printed DIY filter holder

Fig. 6 Case study objects "Green velvet purse" (BK-KOG-29 [38]) and "Purple velvet knife holder" (BK-NM-3086 [39]) from the textile collection of the Rijksmuseum, Amsterdam, The Netherlands

For the purpose of beam filtration we designed an extension to the current FleX-ray Lab setup to have a stable, exact and reproducible way of filtering the X-ray beam. The key idea is to attach a tool on the X-ray tube that enables to place various filters into the beam line. These filters should be held in a fixed position and also the use of multiple filters of different materials and thicknesses should be possible. Therefore, we modelled a beam filter holder for 3D printing, which can be mounted on the tube, and corresponding filter frames in which the filter materials can be clamped in. Similarly to a slide projector these filter frames can then be placed into one of five slits of the beam filter holder. We designed the filter frames so that they are always tightly positioned within the slits and can host filter materials with a thickness ranging between 0.1 and 4.0 mm. The technical drawings can be found in Fig. 5 and the construction files can be made available upon request.

For the processing of the CT data and 3D reconstruction in this article, the FleXbox software [36] was used. First the data was flat- and dark-field corrected using the corresponding recorded dark-fields (D) and flat-fields (F). Each projection image consists of raw photon counts per detector pixel. With the dark-fields we correct for the offset counts of the detector system and the flat-field images are used to normalize pixel-dependent sensitivities of the detector. This way the projection images (P) can be corrected and converted into a beam intensity loss image (I) following the Beer-Lambert law with the following formula:

$$I = \frac{P - D}{F - D} \tag{1}$$

After applying the negative logarithm a reconstruction was obtained using the FDK algorithm [37]. Apart from the flat- and dark-field corrections the data was not post-processed with any computational processing filters to correct/reduce image artifacts. Our purpose in this study is to single out the impact of the different acquisition settings on the image formation.

Experiments and results

In this section we show the influence of different filters and acquisition parameters on the CT image formation and give general guidance on choosing suitable acquisition parameters.

The case studies

To demonstrate the need for an object-tailored acquisition process for cultural heritage objects, we have chosen two case study objects from the textile collection of the Rijksmuseum, Amsterdam, The Netherlands. The objects under investigation were a late sixteenth-century green velvet purse [38] (case study object 1) and an early seventeenth-century purple velvet knife holder [39] (case study object 2) which are shown in Fig. 6. In the following section we will investigate the influence of CT acquisition parameters on the image formation and give general guidance on how to scan these objects. Restricted by the limited time that the cultural heritage objects were available for scanning at our institution we calculated the maximal exposure time available to each scan and kept it at a static value across all scans to be able to conduct all the scans in the different acquisition modes within the available time. Keeping the exposure time constant across different measurements furthermore allowed for

a better comparison between the scans and with this we show the necessity for an object-tailored CT acquisition.

To our knowledge there is currently no suitable framework that would give a good indication of improved image quality for visual interpretation and analysis for cultural heritage objects. As there is no ground truth to compare reconstructions to, and as the interplay between artifacts, noise, and contrast will lead to complications for any quantitative metric such as PSNR, SSIM or MSE, we chose to focus here on qualitative evaluation in the context of the ability to answer specific questions about the object based on the CT-images.

The aim of the CT scans was to uncover information about very thin layers within the objects. Therefore, we chose the full detector resolution with 1911 × 1520 pixels with no hardware binning and used 2881 projections (motivated by the Nyquist-Shannon theorem [40]) for both case studies. All projections have been taken with one frame without averaging. Furthermore, 50 dark- and flat-fields both before and after the scans have been acquired for all case study scans to allow for an adequate pre-processing of the projection data according to formula 1.

To be able to detect very thin layers with our scans we aimed to have a voxel-size within our object of 54.9 µm (green velvet purse) and 45.0 µm (purple velvet knife holder) and positioned the object and detector accordingly. Due to this choice of resolution the objects did not fully fit on the detector in the vertical direction. Therefore, we conducted scans with the detector and source at different heights, to obtain tiled scans of the full object. These were first reconstructed independently and then the resulting volumes were stitched together using the merging capabilities of the FleXbox software [36]. For the velvet purse we used two and for the knife holder four vertical tiles. The total scan time and data size amounted to 163 min and 201.3 GB for the six scans of case study 1 and 138 min and 184.4 GB for the five scans of case study 2.

Case study object 1: "Green velvet purse"

At first sight, this peculiarly shaped object looks like a case for a pair of scissors with a small, leather lined purse on its front with a drawstring. However, the fact that it is not possible to open the case itself complicates probing this hypothesis. Of the three examples surviving in the Netherlands (Rijksmuseum BK-KOG-29, Amsterdam Museum KA-18660, and Oranje-Nassau Museum) two are covered with plain velvet and the third is embroidered with seed pearls and gold thread. Other examples, in France (Musée de Cluny, Paris) and Italy (Bargello, Florence) are similar to the Dutch examples. In the Amsterdam Museum example, three coins were found, one of which dates from 1591, indicating that it might have served as a purse for coins. Besides the function as a scissor-case or purse, the strong resemblance of the object's shape to a phallus makes an erotic connotation possible as well [41].

Through the use of CT scans, we hoped to determine how the purse was made, which materials were used and what gives it its shape. One of our main research questions was whether the object box is empty, indicating it might have been a case, or if there is something inside and if so, what. The answers to these questions can be found in the section *Significance for the image interpretation and analysis of the object*.

The purse has dimensions of roughly 11.0 cm in length, 7.5 cm in width and 3.0 cm in thickness. The materials used are velvet on the exterior with metal eyes on the top, as well as leather lining in the pouch on the front. The velvet is adorned with a drawstring of braided gold thread with a silver core. These metal parts in particular make it difficult to scan and have to be investigated with radiographs to make sure that there is limited photon starvation and that sufficient radiation reaches the detector.

Insights and intuitions on the scan design and acquisition parameter choices.

To determine the minimal photon energy necessary to penetrate the object, we empirically determined the rotation of the scanned object under which we observe the lowest detector counts. This corresponds to the largest attenuation in the line of sight and was found to be in the orientation visible in Fig. 7 where the braided gold/silver wire balls overlay the drawstring outline. In this orientation we increased the tube voltage with steps of 5kV while observing the minimal detector count.

We observed that for tube voltages between 20 and 40 kV the object is not well penetrated resulting in dark/occluded areas where almost no signal was detected behind the object in this line of sight. When using tube voltages above 40 kV we see a sudden increase in the minimal count which implies that a minimal photon energy of 40/45 keV is needed to penetrate all regions of the object in this orientation and in the current configuration of Source-Object-Distance (SOD) and Source-Detector-Distance (SDD). Simultaneously, we observed that without filtration the detector is saturated for a tube voltage of 50 kV and a tube current of 1000 µ*A*.

Furthermore, we reviewed the material composition of the scanned object, i.e. silver and gold, and their main K-edges lie at 25.51 keV and 80.72 keV. To exclude these photon energies, the tube voltage should be set below 80 kV and the filtration should be chosen such that it filters out all photons below an energy of e.g. 30 keV to exclude the silver K-edge. We point out that a tube voltage of 80kV is low for these materials and realize that

Table 1 Acquisition parameters of the scan of case study 1: "Green velvet purse"

	Scan 1	Scan 2	Scan 3	Scan 4	Scan 5	Scan 6
Beam parameters						
Tube voltage	50 kV	50 kV	75 kV	75 kV	75 kV	75 kV
Tube current	700 µA	700 µA	200 µA	1000 µA	1000 µA	1000 µA
Filters	None	Al 0.5 mm	None	Cu 0.5 mm	Sn 0.25 mm	Sn 0.25 mm Cu 0.5 mm Al 0.5 mm
Camera settings						
Exposure time	200 ms					
Nr. of projections	2881					
Nr. of averages	1					
Geometry						
Source-Object-Distance (SOD)	447 mm					
Source-Detector-Distance (SDD)	609 mm					
Object voxel size	54.9 µm					

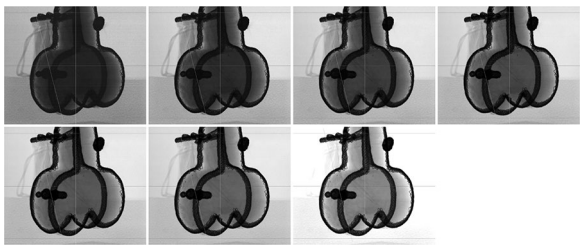

Fig. 7 From left to right, top to bottom: Radiographs of the "Green velvet purse" with different tube voltages between 20kV and 50kV in 5kV steps with the same tube current (1000 µA), same exposure time (200 ms) and no filtration

such low tube voltages are a limiting factor for penetrating thick layers of metal but for our particular CT-system the tube voltages available are bound by regulatory requirements. However, thin layers of metal as presented by the case study objects can also be penetrated with the available tube voltages and enabled still acceptable results. With higher tube voltages it might then be advisable to filter out photons with an energy lower than e.g. 85 keV.

To give the readers of this work insights and intuitions on how different choices of acquisition parameters would influence the resulting radiographs and reconstructions we designed in total six CT scans for the "Green velvet purse". The six conducted scans include two untailored and unfiltered acquisitions, three single-material filtered CT scans as well as one with a Thoraeus compound filter.

For the untailored scans a standard choice simply based on the radiographs and the measured detector signal would result in an unfiltered scan with a tube voltage of 50 kV and a tube current of 700 µA. A second choice aiming for better object penetration would be choosing a higher tube voltage of 75 kV as well as a reduced tube current of 200 µA to avoid saturation of the detector.

For the filtered scans common filter choices would for example be thin sheets of aluminum filtration to filter out very low-energy photons [42] or to use small amounts of copper or tin filtration at higher tube voltages. Lastly, we conducted a scan with a Thoraeus compound filter. To have enough signal we set the maximal tube current of 1000 µA for all of them.

The case study object has not been moved between the different acquisitions to avoid the necessity to register the reconstructed image volumes. If the object would have been moved between the scans a registration of the image volumes would be necessary to be able to compare the scans directly with each other since the orientation of the 2D slices might be slightly different. Therefore, the acquisition parameters were changed digitally and the replacement of the chosen filtration was carried out very carefully avoiding to touch the scanned object. All scans have been conducted in the "High Power"-mode of the FleX-ray scanner which uses a focal spot size below 45 micrometer for operations up to 90W [34]. The exposure time selected for all the scans was limited by the total available scanning time and had to be restricted to a static value of 200 ms. All other details of the scan settings for this case study that we selected for illustrative purposes can be found in Table 1.

Furthermore, all six corresponding beam spectra used for scanning the case study 1: "Green velvet purse" can be found in Fig. 3. The main insight from this is that the mean photon energy in the spectra shifts continuously to higher energies from $\sim$ 25 keV to $\sim$ 60 keV from scan 1 to scan 6. This means that a higher fraction of the X-ray photons within the beam spectra have sufficient energy

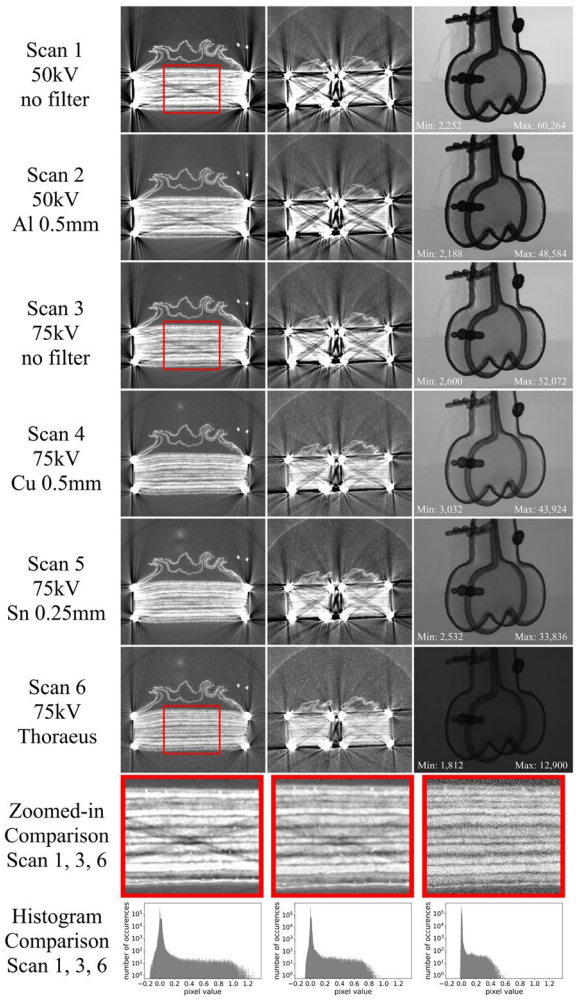

Fig. 8 From left to right, top to bottom: Two reconstruction cross-sections and one radiograph for all six conducted scans of the "Green velvet purse" with the specific acquisition parameters listed in Table 1. The cross-section images shown are taken from slice 1698 and slice 2108. Additionally, comparisons of zoomed-in regions and histograms of scan 1, 3, and 6 of slice 1698 illustrate the improved quality of the object-tailored scan 6

to be able to penetrate the object and that dependent on the chosen filtration the severity of photon starvation artifacts will be reduced.

Radiographs and reconstructions of case study 1: "Green velvet purse".

In the following section we will show radiographs and the reconstructions of these six CT scans and analyse them. In Fig. 8, two horizontal cross-section slices from the reconstruction at different heights in the object and the radiographs of all the different scans (1–6) are presented. We have selected these two cross-sections because they show two levels of severity of the beam hardening and metal artifacts. Once caused by four and once by eight metal trimmings visible in the slices.

In the radiographs for the different acquisition parameters it is visible that changing the tube voltage from 50 kV to 75 kV led to an increased object penetration. Adding aluminum filtration decreased the overall signal but there is no other change in the radiograph observable. Adding stronger filtration leads to less occlusion in the radiograph, which remains only noticeable where multiple metal parts of the velvet purse overlap in the line of sight. However, it also significantly decreases the number of counts and the radiographs appear darker and noisier. The shown projection images have not been adjusted in brightness/contrast level to visually illustrate the decreasing detected signal. Therefore, it is hard to see that there is an increased penetration of the metallic parts of the velvet purse. In the reconstruction the increased penetration of the object can be observed more clearly and how this helps the analysis of the object.

Analysing the reconstruction slices shows an overall image quality improvement from scan 2 towards scan 6. Adding aluminum filtration shows almost no visible difference. The reconstructions of the scans with 75 kV tube voltage show a better penetration of the object but with no filtering there are severe beam hardening and metal image artifacts visible in the cross-sections. With increasing filtering these image artifacts decrease while the noise level rises. Finally, scan 6 has almost no image artifacts within the purse and only small and reduced image artifacts on the corner trimmings. This can be explained by the fact that the minimal photon energy necessary to penetrate the object was determined to be 40/45 keV and the chosen Thoraeus filtration filters out photons with energies between $1.5\,\text{keV} \leq E_{phot} \leq 40\,\text{keV}$. For the second slice with eight metal trimmings the image artifacts within the left and right part of the purse are almost fully removed but in the middle still heavy image artifacts can be observed. This is due to the overlap of multiple metal trimmings in the line of sight for most of the projection images. Although scan 6 exhibits a higher noise level and even shows beginning ring artifacts due to very low detector signal, the reconstruction cross-section slices provide more interpretable information for the cultural heritage object's analysis because of the limited beam hardening and photon starvation artifacts. This is also visible in the histograms of the reconstructed slices (cf. Fig. 8) which show that less pixels have negative or very high values in comparison to the majority of the pixels in the object-tailored scan 6. With more available scanning time the noise level can be compensated by increasing the exposure time but could not be done for our experiments because of time restrictions regarding the scanning of the cultural heritage objects.

Significance for the image interpretation and analysis of the object.

Through the object-tailored CT scan (scan 6), in which the shadows caused by the metal thread trimmings were filtered out, it was possible to closely examine the interior of the purse. In both the unfiltered and filtered reconstructions, it became clear that the purse itself is not hollow, but instead stuffed with several layers of a certain material. Counting the layers and identifying the material of this stuffing was complicated in the unfiltered scan, due to the image artifacts introduced by beam hardening. In the filtered reconstruction, it was possible to identify 11 layers of a non-woven material. The fact that this material showed irregular thicknesses, no evidence of weaving, and no different properties on its different sides, as would be the case for leather, strongly suggest that felt was used.

It was possible to identify a leather lining on the pouch on the front of the object. The CT scan, however, clearly revealed that this lining was only attached at the top and bottom of the pouch, and detached throughout the rest of the pouch (cf. Fig. 8). The velvet is furthermore damaged in certain parts, and repaired with a paper-like material with a matching green colour.

The object-tailored CT scan allowed through its artifact reduction for an easier analysis of the cultural heritage object, for the identification of the filler material based on its structural characteristics as well as provided insights into its build-up. While it was possible to disprove the hypothesis of the purse being hollow and made for holding scissors or other small objects, its precise use remains unknown for now.

Case study object 2: "Purple velvet knife holder"

This early seventeenth-century purple velvet knife holder is elaborately decorated with gold and silver embroidery, and freshwater seed pearls in floral motifs. The removable cap reveals golden decorations of two hands holding a flaming heart and three internal compartments, the contents of which are unfortunately lost. The question arises what it could have contained, besides presumably a knife and a fork, the case being too narrow to contain a spoon unless quite small and shallow. The materials used, and type of decorations present, are reminiscent of a contemporaneous pouch at the Rijksmuseum (BK-NM-11110).

The CT scan was conducted to investigate the construction and material composition of the velvet knife holder. The shape and depth of the third cavity might provide insight into what kind of third object the case once held. Additionally, we wanted to discover if the textile was pre-embroidered and how it was attached to the case. The answers to these questions can be found in the section *Significance for the image interpretation and analysis of the object*.

The Rijksmuseum knife holder has dimensions of roughly 22.0 cm in length, a maximum of 3.4 cm in width and a maximum of 2.5 cm in thickness. The relevant materials used are paper or wood in its interior, with a velvet exterior decorated with gold and silver thread as well as small pearls.

Insights and intuitions on the scan design and acquisition parameter choices.

For this second case study object, the availability of prior information of scanning a similar object (case study object 1) in terms of materials (velvet, leather, gold/silver threads) simplified the scan design process. In contrast, the dimensions of this object were a bit different. A reconstruction with a standard, untailored parameter selection, which exhibits severe image artefacts, was already shown in Fig. 1. Here, we will focus on the importance of choosing the correct rotation and the trade-off regarding the fine tuning of the tube voltage. The impact of the different parameter choices will be shown with the corresponding beam spectra, radiographs and reconstructions.

The purpose of the radiographs shown in Fig. 9 is to illustrate the importance of quantitatively determining the respective minimal count that corresponds to the largest attenuation in the line of sight. Although it might be non-intuitive the 0 degree position is causing a higher attenuation than the one in the 90 degree position. Without determining this rotational position there might be lines of sight where the object is not penetrated sufficiently. This can lead to image artifacts due to photon starvation.

After finding this rotational position we determined the minimal photon energy needed to penetrate the object again. We observed that the needed minimal photon energy is 35/40 keV and that with no filtration for a tube voltage of 60 kV our detector was already saturated. For a tube voltage of 50 kV we saw sufficient minimal detector signal when not taking the object's characteristics into account. But with prior knowledge from the previous case study we decided again to use a "Thoraeus filter" and to stay below a tube voltage of 80 kV because of the K-edges of gold.

To illustrate the trade-off between the reduction of beam hardening image artifacts, improved contrast, and reduced noise we designed four CT scans with identical acquisition parameters which only differ in their respective tube voltage (see Table 2). To have enough signal we had to choose the maximal tube current of 1000 µA for all of them. The exposure time selected for all the scans was limited by the total available scanning time and had to be restricted to a static value of 200 ms

Table 2 Acquisition parameters of the scans of case study 2: "Purple velvet knife holder"

	Scan 1	Scans 2–5
Beam parameters		
Tube voltage	50 kV	60/65/70/75 kV
Tube current	500 μA	1000 μA
		Sn 0.25 mm
		Cu 0.5 mm
Filters	None	Al 0.5 mm
Camera settings		
Exposure time	200 ms	
Nr. of projections	2881	
Nr. of averages	1	
Geometry		
Source-Object-Distance (SOD)	234 mm	
Source-Detector-Distance (SDD)	389 mm	
Object voxel size	45.0 μm	

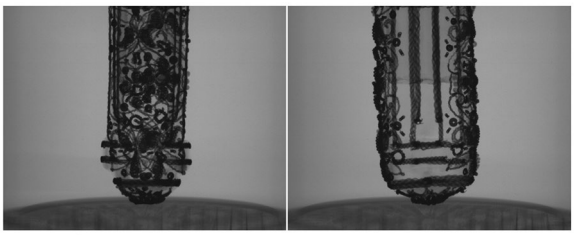

Fig. 9 Radiographs of the 0 degree and 90 degree position of the knife holder with same tube voltage (35 kV), the same tube current (1000 μA), same exposure time (100 ms) and no filtration

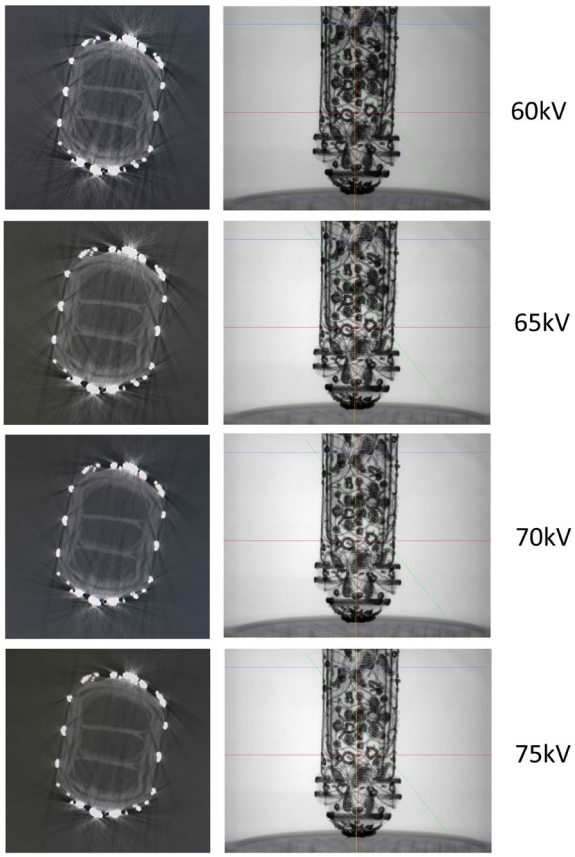

Fig. 10 From top to bottom: Reconstruction slices and radiographs of the "Purple velvet knife holder" of scans 2–5 with the specific acquisition parameters listed in Table 2.The cross-section images shown are taken from slice 1084

The impact of the different parameter choices can be already seen in the corresponding beam spectra in Fig. 3 and will be described and illustrated in more detail in the radiographs and reconstructions in Fig. 10. When looking at the four different beam spectra it can be seen that three important changes are introduced: (i) The change of the maximal photon energy in the spectrum; (ii) the change of the mean photon energy in the spectrum; (iii) the change in overall intensity of the beam. This will influence the penetration of the X-ray photons in the object, the contrast of the images, and the overall SNR.

Radiographs and reconstructions of case study 2: "Purple velvet knife holder".

In Fig. 10 we show the results of our investigation trying out different tube voltages between 60 and 75 kV while keeping all other acquisition parameters the same. This was done since for many materials common in cultural heritage the absorption curve has a steeper slope for lower photon energies. This leads to higher contrast between the different materials. The radiographs in Fig. 10 show, similarly to the beam spectra in Fig. 3, that with lower tube voltage also the overall signal decreases which makes the radiographs a bit more noisy. For tube voltages of 60 or 65 kV the signal measured by the detector is very low and is even close to the dark currents of our detector.

At the same time the change of tube voltage influences the extent of the beam hardening image artifacts due to the shift of the mean and maximal photon energy in the beam spectrum. Whereas for scans 4 and 5 there are almost no image artifacts present in the inside of the object, scans 2 and 3 show more dominant image artifacts. Also, the beam hardening image artifacts in the cavities close to the outer casing are more prominently visible for these two. Nevertheless, there is an increased contrast noticeable between the different materials. This shows that there is a trade-off between having less image artifacts, improved contrast and reduced noise. Scan 4 exhibits a reduction of beam hardening effects with overall acceptable noise as well as contrast levels and

was found qualitatively the best trade-off between these objectives.

Significance for the image interpretation and analysis of the object.

A clear improvement is noticeable when comparing the unfiltered reconstruction slices of scan 1 with the filtered reconstruction slice of scan 4. In the scan 1 reconstruction (as presented in Fig. 1), features of the inner structure are hard to interpret as a result of the image artifacts introduced by beam hardening. In the scan 4 reconstruction, however, these features are more well-defined and easier to distinguish.

This difference in scan quality, supplemented with visual observation of the object, allowed us to gain a better understanding of the materials used and the construction of the object. The three compartments are separate cylindrical shapes, made from (possibly stiffened) paper, that are inserted into a leather outer shell that holds them together. The velvet exterior is attached to this leather outer shell, presumably using glue. The middle cylinder, or cavity, gets pressed together by the adjoining cavities, as the case gets narrower towards its bottom. The shape of the cavities did not give any indications on what the third object could have been that the knife holder once held. The crisp features of the filtered reconstruction allowed us to investigate whether the leather outer shell had any holes, indicating that the exterior was embroidered after attaching it to the object. As no holes were found, however, we concluded that the pearls and floral motifs were applied to the velvet prior to it being glued to the object. The golden plated strips running along the sides of the case covering the seams could perhaps be added after application, as these are most likely glued onto the velvet as opposed to being stitched.

General concept of steps to design an object-tailored CT scan

With the insights and intuitions we gained while investigating the two case study objects, testing various acquisition parameters and observing their influence on the CT image formation, we reflected on a general concept of steps for designing an object-tailored CT scan. Although all investigations were carried out for a specific CT system as well as specific objects and need to be optimized for individual cases, the following seven steps can guide cultural heritage professionals through the process of finding suitable CT acquisition parameters:

1 Determine a suitable SOD and SDD to achieve the desired resolution in the CT reconstruction of the object under investigation. Please be aware that a later change in the tube current or exposure parameters might affect the focal spot size and reduce your resolution.
2 Empirically determine the rotational position with the lowest detector signal which corresponds to the largest attenuation in the line of sight.
3 Investigate the minimal photon energy needed to penetrate the object in this rotational position by slowly increasing the tube voltage while observing the minimal detector signal.
4 Choose adequate filtration that can filter out the low energy part of the spectrum.
5 Exclude the K-edges of any metals within the object by adjusting the tube voltage accordingly.
6 Calculate the maximal feasible acquisition time per projection image of the detector from the total available scanning time to achieve the highest SNR that satisfies the given time and saturation constraints. Also, consider taking multiple frames for averaging each projection, if the total available scanning time allows for that.
7 Find a balance for the trade-off between the reduction of beam hardening image artifacts, improved contrast, and reduced noise by adjusting the tube voltage and tube current within the given boundaries.

Discussion and conclusion

In this study we have introduced how the multi-material nature of cultural heritage objects exhibit challenges for CT scanning and presented several key factors that influence CT image formation. We addressed their underlying physics and discussed how the concept of beam filtration can improve the image quality of CT scans. Illustrated on two case study objects the influence of CT acquisition parameters was investigated and we gave general guidance on how to design a CT scan and how to choose suitable acquisition parameters. We showed that an object-tailored CT acquisition of two case study objects yielded a clear image quality improvement and helped the cultural heritage experts in their analysis. Lastly, we extracted a general concept of steps for museum professionals to design an object-tailored CT scan for individual cases.

Despite the clear image quality improvement of this object-tailored method compared to an untailored CT acquisition, the main disadvantages are firstly that through the filtering the beam intensity is reduced, which results in a decreased SNR, and secondly that the beam hardening problem cannot be completely eliminated [29]. To counter the degraded X-ray signal and greater image noise, longer exposure times and averaging can be used [43]. Depending on the available scanning time and capabilities of the

scanning facility these disadvantages can therefore be mitigated. Overall, the object-tailored choice of acquisition parameters can help though to produce a cleaner image by absorbing the lower energy photons that do not reach the detector and that tend to scatter more. The beam filtration also enables the use of a higher voltage, current and longer exposure times since it prevents the X-ray detector to become saturated through the low-energy photons in the beam spectrum.

The results presented in this manuscript are of course for a specific CT system as well as specific objects and need to be tailored to new individual cases. With the concept of steps for an object-tailored CT scan design we provided a short guidance for this, while the two case studies provide insights and intuitions on choosing suitable acquisition parameters that take the objects' characteristics into consideration and improve image quality in CT reconstructions.

Abbreviations

CT:	Computed tomography
DIY:	Do-it-yourself
CNR:	Contrast-to-noise ratio
SNR:	Signal-to-noise ratio
CMOS:	Complementary metal-oxide semiconductor
FDK:	Feldkamp-Davis-Kress
SOD:	Source-object-distance
SDD:	Source-detector-distance
PSNR:	Peak signal-to-noise ratio
SSIM:	Structural similarity index measure
MSE:	Mean squared error

Acknowledgements

We would like to thank Minnie Middelberg for the photographic documentation of the scanning processes and the scanned cultural heritage objects. We appreciate the help of Mattijs Bakker from the Technologiecentrum of the University van Amsterdam regarding the design and 3D-printing of the beam filtration setup. We thank Dr. Willem Jan Palenstijn for assisting with the computational methods. We are grateful to TESCAN-XRE NV for their collaboration and support regarding the FleX-ray Laboratory.

Author contributions

MBK conceptualized this project and wrote the original draft of the manuscript. FGB and SM assisted in the set-up and scanning of the cultural heritage objects. FGB carried out the CT reconstructions of the objects. SM and PJCvL provided the insights and analysis from the cultural heritage perspective for this publication. FGB, PJCvL, FL, TvL, KJB reviewed and edited the manuscript. All authors read and approved the final manuscript.

Funding

M.B.K. was supported by the Dutch Research Council (NWO, project number OCENW.KLEIN.285). P.J.C.v.L. was supported by a Small Project grant for the IntACT project from the Netherlands Institute for Conservation, Art and Science (NICAS). F.G.B was supported by the Impact4Art project, which is funded by NICAS and the Dutch Research Council (NWO) (Project Number 628.007.033). F.L. was supported by NWO (Project Number 613.009.106). The FleX-ray Laboratory is supported by NWO (project number 639.073.506). The sponsors were not involved in the research and writing process.

Availability of data and materials

The datasets generated and/or analysed during the current study are not publicly available due to the excessive size of 386GB but are available from the corresponding author on reasonable request.

Declarations

Competing interests

The authors declare that they have no competing interests.

Received: 13 March 2023 Accepted: 7 June 2023
Published online: 19 June 2023

References

1. Hsieh J. Computed tomography: principles, design, artifacts, and recent advances. Washington: SPIE press; 2003.
2. Hansen PC, Jørgensen J, Lionheart WRB. Computed tomography: algorithms, insight, and just enough theory. Soc Ind Appl Math. 2021. https://doi.org/10.1137/1.9781611976670.
3. Villarraga-Gómez H, Herazo E, Smith S. X-ray computed tomography: from medical imaging to dimensional metrology. Precis Eng. 2019;60:544–69. https://doi.org/10.1016/j.precisioneng.2019.06.007.
4. Casali F. Chapter 2 x-ray and neutron digital radiography and computed tomography for cultural heritage. Physical techniques in the study of art, archaeology and cultural heritage. Amsterdam: Elsevier; 2006. p. 41–123.
5. Domínguez-Delmás M, Bossema FG, Van der Mark B, Kostenko A, Coban SB, Van Daalen S, Van Duin P, Batenburg KJ. Dating and provenancing the woman with lantern sculpture - a contribution towards attribution of netherlandish art. J Cult Herit. 2021;50:179–87.
6. Bossema FG, Domínguez-Delmás M, Palenstijn WJ, Kostenko A, Dorscheid J, Coban SB, Hermens E, Batenburg KJ. A novel method for dendrochronology of large historical wooden objects using line trajectory x-ray tomography. Sci Rep. 2021;11:11024.
7. Re A, Albertin F, Avataneo C, Brancaccio R, Corsi GJ, ad Cotto, De Blasi S, Dughera G, Durisi E, Ferrarese W, Giovagnoli A, Grassi N, Lo Giudice A, Mereu P, Mila G, Nervo M, Pastrone N, Prino F, Ramello L, Ravera M, Ricci C, Romero A, Sacchi R, Staiano A, Visca L, Zamprotta L. X-ray tomography of large wooden artworks the case study of "doppio corpo" by pietro piffetti. Herit Sci. 2014;2:19.
8. Vandenbeusch M, O'Flynn BD, Moreno ABD. Layer by layer: the manufacture of graeco-roman funerary masks. J Egypt Archaeol. 2021;107:281–98.
9. Fried P, Woodward J, Brown D, Harvell D, Hanken J. 3d scanning of antique glass by combining photography and computed tomography. Digit Appl Archaeol Cult Herit. 2020;18:00147.
10. Sodini N, Dreossi D, Giordano A, Kaiser J, Zanini F, Zikmund T. Comparison of different experimental approaches in the tomographic analysis of ancient violins. J Cult Herit. 2017;27:88–92.
11. Dorscheid J, Bossema FG, Van Duin P, Coban SB, Van Liere R, Batenburg KJ, Di Stefano GP. Looking under the skin - multi-scale CT scanning of a peculiarly constructed cornett in the Rijksmuseum. Herit Sci. 2022;10:10.
12. Andonova M. Ancient basketry on the inside: X-ray computed microtomography for the non-destructive assessment of small archaeological monocotyledonous fragments: examples from southeast europe. Herit Sci. 2021. https://doi.org/10.1186/s40494-021-00631-z.
13. Mihanović F, Jerković I, Kružić I, Andjelinović S, Janković S, Bašić Ž. From biography to osteobiography: an example of anthropological historical identification of the remains of st. p aul. Anat Rec. 2017;300(9):1535–46.
14. Macchi V, Picardi E, Porzionato A, Morra A, Tabarin L, Gusella F, Grignon B, Caro R. Friar leopold mandic (1866–1942): the computed tomography of the body of a saint. Surg Radiol Anat. 2018;40:1–9. https://doi.org/10.1007/s00276-018-2050-0.
15. Vandivere A, Wadum J, Van den Berg KJ, van Loon A. From 'vermeer illuminated' to 'the girl in the spotlight': approaches and methodologies for the scientific (re-)examination of vermeer's girl with a pearl earring. Herit Sci. 2019;7:1–14. https://doi.org/10.1186/s40494-019-0307-5.
16. Montaina L, Longo S, Galotta G, Tranquilli G, Saccuman R, Capuani S. Assessment of the panel support of a seventeenth-century dutch painting by clinical multislice computed tomography. Stud Conserv. 2021;66(3):174–81.
17. Wilson P, Smith M, Hay J, Warnett J, Attridge A, Williams M. X-ray computed tomography (xct) and chemical analysis (edx and xrf) used in conjunction for cultural conservation: the case of the earliest scientifically

described dinosaur megalosaurus bucklandii. Herit Sci. 2018. https://doi.org/10.1186/s40494-018-0223-0.
18. Bossema FG, Coban SB, Kostenko A, Van Duin P, Dorscheid J, Garachon I, Hermens E, van Liere R, Batenburg KJ. Integrating expert feedback on the spot in a time-efficient explorative CT scanning workflow for cultural heritage objects. J Cult Herit. 2021;49:38–47.
19. Jansson A, Ekengren J, Zekavat A-R, Pejryd L. Effects of x-ray penetration depth on multi material computed tomography measurements. In: 6t H Conference on Industrial Computed Tomography. 2016.
20. Goldman LW. Principles of CT: radiation dose and image quality. J Nucl Med Technol. 2007;35(4):213–25. https://doi.org/10.2967/jnmt.106.037846.
21. Pan X, Siewerdsen J, La Riviere PJ, Kalender WA. Anniversary paper: development of x-ray computed tomography: the role of medical physics and aapm from the 1970s to present. Med Phys. 2008;35(8):3728–39. https://doi.org/10.1118/1.2952653.
22. Zwanenburg EA, Williams MA, Warnett JM. Review of high-speed imaging with lab-based x-ray computed tomography. Meas Sci Technol. 2021;33(1): 012003. https://doi.org/10.1088/1361-6501/ac354a.
23. Als-Nielsen J, McMorrow D. Elements of modern X-ray physics. Hoboken, NJ: John Wiley & Sons; 2011.
24. Patton JA, Turkington TG. Spect/ct physical principles and attenuation correction. J Nucl Med Technol. 2008;36(1):1–10. https://doi.org/10.2967/jnmt.107.046839.
25. de Casteele EV, Dyck DV, Sijbers J, Raman E. An energy-based beam hardening model in tomography. Phys Med Biol. 2002;47(23):4181. https://doi.org/10.1088/0031-9155/47/23/305.
26. Salamon M, Arzig M, Wellmann PJ, Uhlmann N. Comparison of achievable contrast features in computed tomography observing the growth of a 4h-sic bulk crystal. Materials. 2019;12(22):3652.
27. Meloni A, Frijia F, Panetta D, Degiorgi G, De Gori C, Maffei E, Clemente A, Positano V, Cademartiri F. Photon-counting computed tomography (pcct): technical background and cardio-vascular applications. Diagnostics. 2023. https://doi.org/10.3390/diagnostics13040645.
28. Tarplee MF, Corps N. Acquiring optimal quality x-ray μct scans. Appl note. 2008;1:93–9.
29. Jennings RJ. A method for comparing beam-hardening filter materials for diagnostic radiology. Med Phys. 1988;15(4):588–99.
30. Hamba H, Nikaido T, Sadr A, Nakashima S, Tagami J. Enamel lesion parameter correlations between polychromatic micro-ct and tmr. J Dent Res. 2012;91(6):586–91. https://doi.org/10.1177/0022034512444127. (**PMID: 22476867**).
31. Kim E, Muroi K, Koike T, Kim J. Dose reduction and image quality optimization of pediatric chest radiography using a tungsten filter. Bioengineering. 2022. https://doi.org/10.3390/bioengineering9100583.
32. Khan FM, Gibbons JP. Khan's the physics of radiation therapy. Philadelphia, PA: Lippincott Williams & Wilkins; 2014.
33. XRE TESCAN: TESCAN micro-CT webpage. 2023. https://info.tescan.com/micro-ct Accessed 19 Jan 2023.
34. Coban SB, Lucka F, Palenstijn WJ, Van Loo D, Batenburg KJ. Explorative imaging and its implementation at the flex-ray laboratory. J Imaging. 2020. https://doi.org/10.3390/jimaging6040018.
35. Limited D. X-ray detector product specifications DEXELA 1512 CMOS. 2010. http://file.yizimg.com/344621/2010061015232418.pdf Accessed 7 Apr 2021.
36. Kostenko A, Palenstijn WJ, Coban SB, Hendriksen AA, van Liere R, Batenburg KJ. Prototyping x-ray tomographic reconstruction pipelines with flexbox. SoftwareX. 2020;11: 100364.
37. Feldkamp L, David LC, Kress J. Practical cone-beam algorithm. J Opt Soc Am A. 1984;1:612–9.
38. Rijksmuseum Amsterdam: BK-KOG-29 - Beurs van groen fluweel met trekkoord en afgezet met gouddraad op een doosje in de vorm van een schaar (fallus?) van dito fluweel en passement, voorzien van twee metalen ogen (na 1580). http://hdl.handle.net/10934/RM0001.COLLECT.16209 Accessed 19 Jan 2023.
39. Rijksmuseum Amsterdam: BK-NM-3086 - Langwerpig, taps toelopend foedraal met dop, van leer verdeeld in drie compartimenten, bekleed met paars fluweel en geborduurd met goud- en zilverdraad, zoetwaterparels, en zilveren lovers (c. 1600 - c. 1625). http://hdl.handle.net/10934/RM0001.COLLECT.302027 Accessed 19 Jan 2023.
40. Kharfi F. Mathematics and physics of computed tomography (CT): demonstrations and practical examples. In: Kharfi F, editor. Imaging and radioanalytical techniques in interdisciplinary research. IntechOpen: Rijeka; 2013.
41. Amsterdam museum: KA 18660 - Phallus Beurs (1500 - 1600). http://hdl.handle.net/11259/collection.25592. Accessed 9 Mar 2023.
42. Fried P, Woodward J, Brown D, Harvell D, Hanken J. 3d scanning of antique glass by combining photography and computed tomography. Digit Appl Archaeol Cult Herit. 2020;18:00147. https://doi.org/10.1016/j.daach.2020.e00147.
43. Ketcham RA, Carlson WD. Acquisition, optimization and interpretation of x-ray computed tomographic imagery: applications to the geosciences. Comput Geosci. 2001;27(4):381–400. https://doi.org/10.1016/S0098-3004(00)00116-3.
44. Boas FE, Fleischmann D, et al. Ct artifacts: causes and reduction techniques. Imaging Med. 2012;4(2):229–40.
45. Boone JM, Seibert JA. An accurate method for computer-generating tungsten anode x-ray spectra from 30 to 140 kv. Med Phys. 1997;24(11):1661–70. https://doi.org/10.1118/1.597953.

Publisher's Note